Liu *et al.*
Chinese Journal of Mechanical Engineering (2022) 35:88
https://doi.org/10.1186/s10033-022-00759-4

Chinese Journal of Mechanical Engineering

ORIGINAL ARTICLE

Open Access

Prediction and Analysis of the Force and Shape Parameters in Variable Gauge Rolling

Yuanming Liu[1,2,3*], Zhenhua Wang[1,2,3], Tao Wang[1,2,3], Jie Sun[4], Xianguang Zheng[1], Dianhua Zhang[4] and Qingxue Huang[1,2,3]

Abstract

Variable gauge rolling is a new process to obtain a plate for which the thickness changes continuously by continuously and dynamically adjusting the roll gap upward and downward in the rolling process. This technology is an effective method for producing lightweight, low-cost, and economical plates. However, variable gauge rolling is an unsteady process, and the changes in the force and deformation parameters are complex. In this research, based on the minimum energy theory of the variational principle and considering the characteristics of the roll movement and workpiece deformation comprehensively, the internal plastic deformation, friction, shear and tension powers, and the minimum result of the total power functional in upward and downward rolling are obtained with the first integral and then with a variation of adopting the specific plastic power and strain rate vector inner product. The analytical results of the deformation and force parameters are also established using the variational method. Then the precision of this model is certified using the measured values in a medium plate hot rolling plant and the experimental data for Tailor Rolled Blank rolling. Good agreement is found. Additionally, the variation rule of bite angle, neutral angle, and location neutral points are shown, and the change mechanism of the friction parameter on the stress state effect coefficient is given in variable gauge rolling. This research proposes a new mathematical model for rolling process control that provides a scientific basis and technical support for obtaining an accurate section shape in variable gauge rolling production.

Keywords: Variable gauge rolling, Analytical solution, Roll separating force, Energy method, Neutral point

1 Introduction

Variable gauge rolling is applied to produce plates that have the benefit of being lightweight due to the optimization of the plate thickness according to the load distribution. If traditional equal-thickness steel plates are replaced by variable thickness plates with comparable properties, more than 30% of the steel in the construction of bridges (such as the steel in the main beam flange, and web) can be saved [1], and more than 40% of the weight in the manufacture of automobile parts (such as reinforcement beams, and instrument panel bottom crossbeams) can be reduced [2]. Variable thickness plates obtained by rolling have the advantages of decreased frame weights, reduction of welds, high production efficiency, and yield ratios [3]. Variable thickness plates have been preliminarily applied in automobile manufacturing, construction, shipbuilding bridge industries and so on [4]. The demand for variable thickness plates is growing [5].

There are two different transition zones from the thick area to the thin area and from the thin area to the thick area. The shape and the size of these transition zones not only determine the bearing capacity during service, but also influence the subsequent processing and die design [6]. Nevertheless, the high prediction accuracy force parameters (such as the roll torque, and roll separating force) and deformation parameters (such as the location of the neutral point, and forward slip) for different

*Correspondence: liuyuanming@tyut.edu.cn
[1] College of Mechanical and Vehicle Engineering, Taiyuan University of Technology, Taiyuan 030024, China
Full list of author information is available at the end of the article

processing parameters are the keys to obtaining excellent shapes for the transition zones in variable thickness plates [7, 8].

Variable gauge rolling has been widely used in Mizushima Automatic Plan View Pattern Control System rolling (MAS rolling) [9], Tailor Rolled Blank (TRB) [10], Longitude Profile (LP) hot rolling [11], and Flying Gauge Change (FGC) [12]. To compensate for the irregular shape of the workpiece in medium plate rolling, the MAS rolling method is adopted to improve the shape in the middle pass. Then the medium plate not only reduces the loss of the head, tail, and edges, but it also enhances the metal yield and the yield ratio [13], as shown in Figure 1(a). TRB is used to replace Tailor Welded Blank (TWB), which is obtained by welding two or more plates of different thicknesses together [14]. TRBs are obtained by directly cutting a periodic variable thickness plate produced through flexible rolling technology, as shown in Figure 1(b). TRB has apparent features such as no weld joint, good surface quality, reliable subsequent processing, and high production efficiency, suitability for large-scale production, low production cost, and energy savings [15]. TRB adopts a new processing technology to reduce the weight of structural plates, and meets the performance requirements of the different parts of a vehicle.

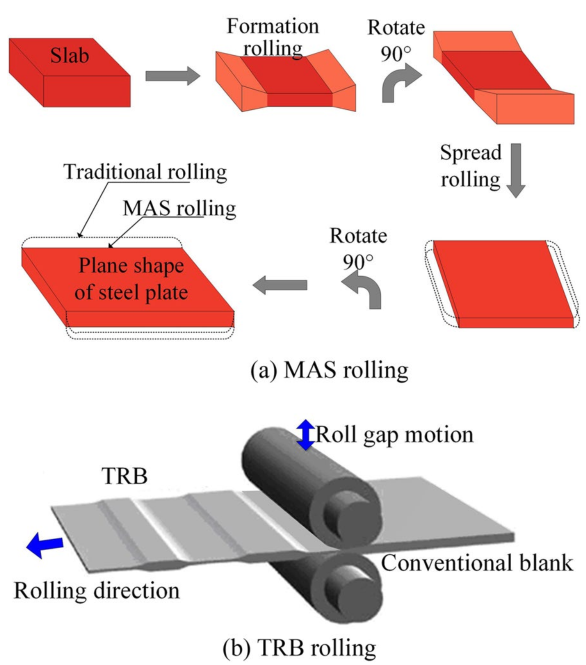

Figure 1 Schematic diagram of typical variable gauge rolling

Therefore, it reduces the bodyweight of vehicles and can be used to research and develop environmentally friendly and energy-saving automobiles.

Ding et al. [16] proposed a method for accurately analyzing and optimizing the shape of the transition zone in TRB based on the isogeometric analysis method. According to the rolling deformation features, Zhi et al. [17] designed four kinds of TRB transition curve functional equations, namely, double arc, straight line, concave arc, and power function equations, and analyzed the roll center trajectory during variable gauge rolling. Wang et al. [18] proposed the design method of transition zone curve, and deduced the velocity models of workpiece's horizontal motion and upward and downward roll motion, but the specific procedure to calculate the neutral angle contained in these velocity models was not given. Wang et al. [12] adopted variable gauge rolling technology in FGC and studied the setting principle of the roll gap and roll circumferential speed. Yu et al. [19] derived the forward slip equation in the variable gauge rolling process according to the equal flow per second, and analyzed the influence of different kinds of transition zone shapes on the forward slip, and compared them with the results of a finite element simulation. Because the deformation characteristics outside the transition zone in variable gauge rolling are similar to the characteristics in traditional rolling, Zhang et al. [20] calculated the rolling speeds in the thick area and the thin area with the traditional rolling theory, and then took the mean value of the two rolling speeds as the speed of the transition zone.

Liu [1] systematically researched the theory and application of variable gauge rolling. The bite condition and the length of the contact arc were analyzed first, and then the formulas of the forward slip and neutral angle were deduced based on the assumption that the unit pressure was uniformly distributed along the contact arc. The changes in the roll separating force were analyzed using the finite element method in variable gauge rolling. Zhang [21] established force equilibrium differential equations in TRB rolling with the slab method, and the unit pressure distribution in the deformation zone was obtained by referring to the idea of solving the Karman differential equation. Then the calculation formulas of the roll separating force, neutral angle, and forward and backward slips were determined. Yu et al. [22] analyzed the fluctuation of roll separating force in variable gauge rolling using finite element software, and researched the influences of the reduction, friction, and radius on the roll separating force.

The exit position of the workpiece is not on the centerline of the two cylindrical work rolls in the variable gauge rolling, so the thickness of the exit zone is not equal to the loaded roll gap. The variable gauge rolling process cannot be identical to the combination of the infinite equal thickness traditional rolling process, and the velocity fields of the two processes are different even if the instantaneous inlet and outlet thicknesses are the same [23]. Therefore, in this research, a velocity field satisfying kinematically admissible conditions is established based on the mass conservation law in the deformation zone with consideration of the influence of the upward and downward motions of the rolls. The high accuracy mechanical and deformation parameters in upward and downward rolling are obtained using suitable mathematical solution methods.

2 Velocity Field

The Cartesian coordinate system is located at the central node of the centerline of the two work rolls. The length, thickness, and width directions of the workpiece are expressed by the x, y, and z axes separately, as shown in Figures 2 and 3. For the work rolls, the original radius is represented by R_0, and the flattened radius is represented by R. The workpiece thickness of the thick zone decreases from $2h_0$ to $2h_{\text{thick}}$, and the thickness of the thin zone is reduced from $2h_0$ to $2h_{\text{thin}}$. The exit thickness of the deformation zone at some point is $2h_1$, so the unilateral reduction is $\Delta h = h_0 - h_1$. v_R is the roll circumferential speed. V_y is the speed of the upward or downward motion of the rolls. θ is the bite angle, and α is the contact angle. α_0 is the wedge angle of the variable thickness section, and x_0 is the distance from the exit to the centerline of the roll.

According to the directions of the Cartesian coordinate system, V_y is a positive value in the upward rolling, and it is a negative value in the downward rolling. To simplify the calculation, this model ignores the influence of spreading, and the width of the workpiece is $2w$. A quarter deformation zone is used to build the model to simplify the calculation due to the symmetry. The expressions for half of the thickness h_x (h_α) of the deformation zone and the first derivative h_x' are described as Eqs. (1)–(4).

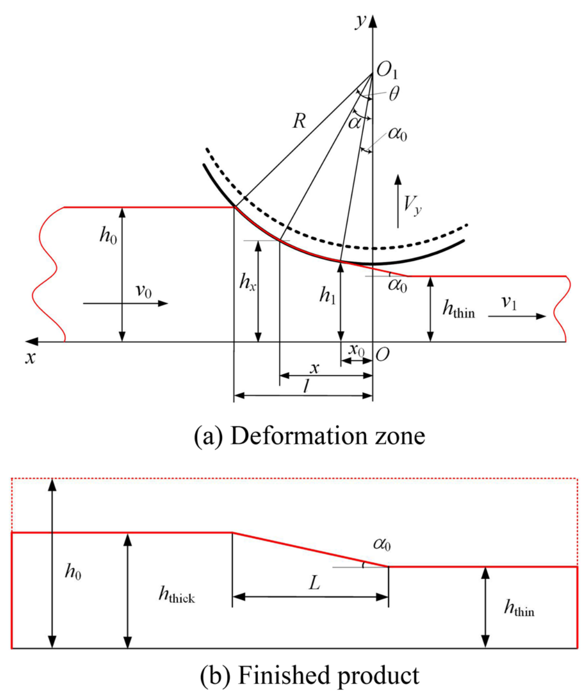

Figure 2 Schematic diagram of the deformation zone and finished product in upward rolling

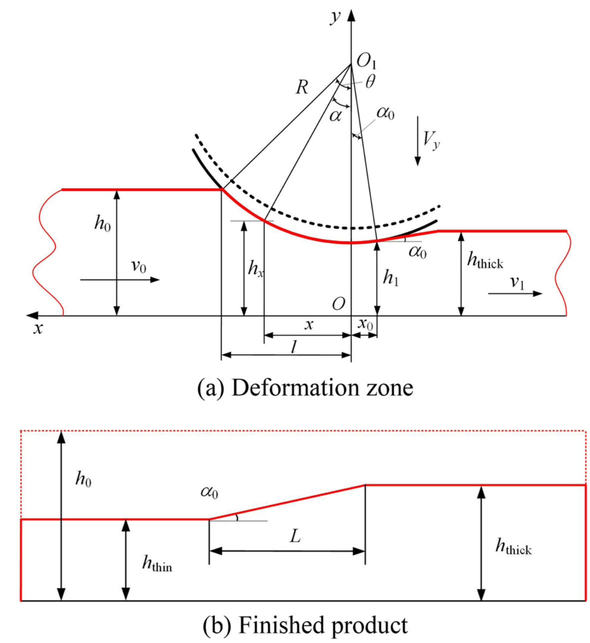

Figure 3 Schematic diagram of the deformation zone and finished product in downward rolling

$$h_x = h_0 + \sqrt{R^2 - l^2} - \sqrt{R^2 - x^2}, \tag{1}$$

$$h_\alpha = h_0 + R\cos\theta - R\sin\alpha, \tag{2}$$

$$x = R\sin\alpha, \mathrm{d}x = R\cos\alpha\mathrm{d}\alpha, \tag{3}$$

$$h_x^{'} = \frac{x}{\sqrt{R^2 - x^2}} = \tan\alpha, \tag{4}$$

Considering the influence of the upward or downward motions of the rolls during variable gauge rolling, the constant volume condition of the metal flow satisfies

$$h_0 v_0 = h_x v_x + V_y R(\theta - \alpha). \tag{5}$$

The velocity components during variable gauge rolling are

$$\begin{cases} v_x = \dfrac{h_0 v_0 - V_y R\theta + V_y R\alpha}{h_x}, \\ v_y = \left(\dfrac{v_x}{h_x}h_x^{'} - \dfrac{V_y R}{x h_x}h_x^{'}\right)y, \\ v_z = 0. \end{cases} \tag{6}$$

The strain rate field components during variable gauge rolling are

$$\begin{cases} \dot{\varepsilon}_x = -\dfrac{v_x}{h_x}h_x^{'} + \dfrac{V_y R}{x h_x}h_x^{'}, \\ \dot{\varepsilon}_y = \dfrac{v_x}{h_x}h_x^{'} - \dfrac{V_y R}{x h_x}h_x^{'}, \\ \dot{\varepsilon}_z = 0. \end{cases} \tag{7}$$

According to Eqs. (6) and (7), at the inlet of the zone: $v_x|_{x=l} = v_0$, $v_y|_{y=0} = 0$, and $v_z|_{z=0} = 0$; and at the exit of the zone: $v_y|_{x=x_0} \neq 0$. This is caused by the upward or downward motions of the rolls. The strain rate field satisfies $\dot{\varepsilon}_x + \dot{\varepsilon}_y + \dot{\varepsilon}_z = 0$, so the velocity field satisfies the velocity boundary condition, and the strain rate field meets the constant volume condition. Eqs. (6) and (7) fulfill the kinematically admissible conditions.

3 Analytical Model of Total Power Functional in Upward Rolling

Because the deformation zones in variable gauge and traditional rolling are different, the expressions for the length of the contact arc l_{total} and the thickness of the exit zone h_1 in the deformation zone during the upward rolling according to Figure 2 are

$$l_{\text{total}} = l - x_0 = \sqrt{R^2 + (R\cos\alpha_0 - \Delta h)^2} - x_0, \tag{8}$$

$$h_1 = h_{\text{hthin}} + V_y t, \tag{9}$$

where t is the time of the variable gauge rolling.

3.1 Internal Plastic Deformation Power

To solve the calculation for the internal plastic deformation power difficulty that is caused by the nonlinear Mises yield criterion, the internal plastic deformation power can be received using the MY liner yield criterion in upward rolling. The MY liner yield criterion is the arithmetic mean of the twin shear stress and Tresca yield criterion loci [24]. Noting that $\dot{\varepsilon}_{\max} = \dot{\varepsilon}_x$, $\dot{\varepsilon}_{\min} = \dot{\varepsilon}_y$ in Eq. (7) and the internal plastic deformation power $\dot{W}_{\text{ui}}$ is

$$\begin{aligned} \dot{W}_{\text{ui}} &= \int_V D(\dot{\varepsilon}_{ij})\mathrm{d}V = \frac{16}{7}\sigma_{\text{s}} \int_{x_0}^{l}\int_0^w\int_0^{h_x} (\dot{\varepsilon}_{\max} - \dot{\varepsilon}_{\min})\mathrm{d}x\mathrm{d}y\mathrm{d}z \\ &= -\frac{32}{7}\sigma_{\text{s}} w \int_{x_0}^{l}\left[\left(-h_0 v_0 + V_y R\theta\right)\frac{h_x^{'}}{h_x} - V_y R\frac{\alpha}{h_x}h_x^{'} + V_y R\frac{h_x^{'}}{x}\right]\mathrm{d}x. \end{aligned} \tag{10}$$

To simplify the calculation and writing, it is assumed that $M = h_0/R + \cos\theta$. The metal flow volume per second is $U = v_0 h_0 w = v_n h_n w = v_R\cos\alpha_N w(h_0 + R\cos\theta - R\cos\alpha_n)$. Therefore, the mean value of $\cos\alpha$ obtained with the integral mean value theorem is

$$\overline{\cos\alpha} = \frac{\int_{\alpha_0}^{\theta}\cos\alpha\mathrm{d}\alpha}{\theta - \alpha_0} = \frac{\sin\theta - \sin\alpha_0}{\theta - \alpha_0}. \tag{11}$$

The internal plastic deformation power $\dot{W}_{\text{ui}}$ is finally obtained as

$$\dot{W}_{\mathrm{ui}}=\frac{32}{7}\sigma_{\mathrm{s}}U\ln\frac{h_0}{h_1}+\frac{32}{7}\sigma_{\mathrm{s}}wV_yR\left\{\theta\ln\frac{h_1(M-\cos\theta)}{h_0}-\alpha_0\ln\left(M-\cos\alpha_0\right)-(\theta-\alpha_0)\left[1+\ln\left(M-\frac{\sin\theta-\sin\alpha_0}{\theta-\alpha_0}\right)\right]\right\}. \tag{12}$$

3.2 Shear Power

According to the velocity field in Eq. (6), the velocity discontinuity at the inlet of the zone ($x=l$) is

$$\begin{cases} v_y|_{x=l}=\left(\dfrac{v_0}{h_0}-\dfrac{V_yR}{lh_0}\right)\tan\theta y,\\ v_z|_{x=l}=0. \end{cases} \tag{13}$$

Therefore, the shear power $\dot{W}_{\mathrm{us1}}$ at the inlet of the zone is

$$\begin{aligned}\dot{W}_{\mathrm{us1}}&=4k\int_0^{h_0}\int_0^{w}|\Delta v_{\mathrm{t}}|\mathrm{d}y\mathrm{d}z\\&=4k\int_0^{h_0}\int_0^{w}\left(\frac{v_0}{h_0}-\frac{V_yR}{lh_0}\right)\tan\theta y\mathrm{d}y\mathrm{d}z\\&=2kwh_0\tan\theta\left(v_0-\frac{V_yR}{l}\right)\\&=2kU\tan\theta-\frac{2kwh_0V_yR\tan\theta}{l}.\end{aligned} \tag{14}$$

At the exit of the zone ($x=x_0$)

$$\begin{cases} v_y\big|_{x=x_0}=\left(\dfrac{h_0v_0-V_yR\theta+V_yR\alpha_0}{h_1^2}-\dfrac{V_yR}{x_0h_1}\right)\tan\alpha_0y,\\ v_z|_{x=x_0}=0. \end{cases} \tag{15}$$

Hence, the shear power $\dot{W}_{\mathrm{us2}}$ at the exit of the zone is

$$\begin{aligned}\dot{W}_{\mathrm{us2}}&=4k\int_0^{h_1}\int_0^{w}\left|\left(\frac{h_0v_0-V_yR\theta+V_yR\alpha_0}{h_1^2}-\frac{V_yR}{x_0h_1}\right)\tan\alpha_0y\right|\mathrm{d}y\mathrm{d}z\\&=2kU\tan\alpha_0-2kwV_yR\tan\alpha_0\left(\frac{h_1}{x_0}+\theta-\alpha_0\right).\end{aligned} \tag{16}$$

Then the total shear power is

$$\dot{W}_{\mathrm{us}}=\dot{W}_{\mathrm{us1}}+\dot{W}_{\mathrm{us2}}=2kU(\tan\theta+\tan\alpha_0)-\frac{2kwh_0V_yR\tan\theta}{l}-2kwV_yR\tan\alpha_0\left(\frac{h_1}{x_0}+\theta-\alpha_0\right). \tag{17}$$

3.3 Friction Power

The friction only exists on the contact surface between the roll and the workpiece, as indicated in Figure 2. According to Eq. (6), the tangential velocity discontinuity Δv_f on the contact surface along the x, y, and z axes is Δv_x, Δv_y, and Δv_z, respectively.

$$\begin{cases} \Delta v_x=v_R\cos\alpha-\left(\dfrac{h_0v_0-V_yR\theta}{h_x}+\dfrac{V_yR\alpha}{h_x}\right),\\ \Delta v_y\big|_{y=h_x}=v_R\sin\alpha-V_y-\left(\dfrac{h_0v_0-V_yR\theta}{h_x}+\dfrac{V_yR\alpha}{h_x}-\dfrac{V_yR}{x}\right)\tan\alpha,\\ \Delta v_z=0. \end{cases} \tag{18}$$

The tangential velocity discontinuity Δv_{f} and the friction stress $\tau_{\mathrm{f}}=mk$ are collinear vectors, so the friction power $\dot{W}_{\mathrm{uf}}$ is calculated using the co-line vector inner product in the whole deformation zone [25]. It is found that

$$\begin{aligned}\dot{W}_{\mathrm{uf}}&=4\int_{x_0}^{l}\int_0^{w}\boldsymbol{\tau}_{\mathrm{f}}\Delta\boldsymbol{v}_{\mathrm{f}}\mathrm{d}F=4\int_{x_0}^{l}\int_0^{w}(\tau_{\mathrm{fx}}\Delta v_x+\tau_{\mathrm{fy}}\Delta v_y+\tau_{\mathrm{fz}}\Delta v_z)\mathrm{d}F\\&=4mk\int_{x_0}^{l}\int_0^{w}(\Delta v_x\cos\alpha+\Delta v_y\cos\beta+\Delta v_z\cos\gamma)\sec\alpha\mathrm{d}x\mathrm{d}z,\end{aligned} \tag{19}$$

where $\cos\alpha$, $\cos\beta$ and $\cos\gamma$ are the direction cosines, the values of which can be determined by using Eq. (1) [26].

$$\cos\alpha=\pm\frac{\sqrt{R^2-x^2}}{R},\ \cos\gamma=\pm\frac{x}{R}=\sin\alpha,\ \cos\beta=0. \tag{20}$$

Substituting Eqs. (18) and (20) into Eq. (19) yields

$$\begin{aligned}
\dot{W}_{\mathrm{uf}} &= 4mkw\left(\int_{x_0}^{l}\Delta v_x\cos\alpha\sec\alpha\,\mathrm{d}x+\int_{x_0}^{l}\Delta v_y\sin\alpha\sec\alpha\,\mathrm{d}x\right)\\
&= 4mkw\left\{\int_{x_0}^{l}\left[v_R\cos\alpha-\left(\frac{h_0v_0-V_yR\theta}{h_x}+\frac{V_yR\alpha}{h_x}\right)\right]\mathrm{d}x\right.\\
&\quad\left.+\int_{x_0}^{l}\left[v_R\sin\alpha-V_y-\left(\frac{h_0v_0-V_yR\theta+V_yR\alpha}{h_x}-\frac{V_yR}{x}\right)\tan\alpha\right]\tan\alpha\,\mathrm{d}x\right\}\\
&= 4mkw\left(\int_{x_0}^{l}\mathrm{B}_{\mathrm{I1}}\mathrm{d}x+\int_{x_0}^{l}\mathrm{B}_{\mathrm{I2}}\mathrm{d}x\right)=4mkw(\mathrm{I}_1+\mathrm{I}_2),
\end{aligned} \tag{21}$$

where I_1 is

$$\begin{aligned}
\mathrm{I}_1 &= \int_{x_0}^{l}\mathrm{B}_{\mathrm{I1}}\mathrm{d}x=-\int_{x_0}^{x_n}\mathrm{B}_{\mathrm{I1}}\mathrm{d}x+\int_{x_n}^{l}\mathrm{B}_{\mathrm{I1}}\mathrm{d}x\\
&= v_RR\left(\frac{\alpha_0}{2}+\frac{\theta}{2}-\alpha_n+\frac{\sin 2\theta}{4}-\frac{\sin 2\alpha_n}{2}+\frac{\sin 2\alpha_0}{4}\right)+(h_0v_0-V_yR\theta+\\
&\quad V_yR\alpha_m)\left\langle\alpha_0+\theta-2\alpha_n+\frac{2M}{\sqrt{M^2-1}}\left\{2\arctan\left[\sqrt{\frac{M+1}{M-1}}\tan\left(\frac{\alpha_n}{2}\right)\right]-\arctan\left[\sqrt{\frac{M+1}{M-1}}\tan\left(\frac{\alpha_0}{2}\right)\right]-\arctan\left[\sqrt{\frac{M+1}{M-1}}\tan\left(\frac{\theta}{2}\right)\right]\right\}\right\rangle,
\end{aligned} \tag{22}$$

where the mean value of the contact angle α_m during upward rolling is obtained with the integral mean value theorem

$$\alpha_m=\frac{\int_{x_0}^{l}\alpha\,\mathrm{d}x}{l-x_0}=\frac{\theta\sin\theta+\cos\theta-\alpha_0\sin\alpha_0-\cos\alpha_0}{\sin\theta-\sin\alpha_0}. \tag{23}$$

Similarly,

$$\begin{aligned}
\mathrm{I}_2 &= \int_{x_0}^{l}\mathrm{B}_{\mathrm{I2}}\mathrm{d}x=-\int_{x_0}^{x_n}\mathrm{B}_{\mathrm{I2}}\mathrm{d}x+\int_{x_n}^{l}\mathrm{B}_{\mathrm{I2}}\mathrm{d}x\\
&= v_RR\left(\frac{\alpha_0}{2}+\frac{\theta}{2}-\alpha_n+\frac{\sin 2\alpha_n}{2}-\frac{\sin 2\theta}{4}-\frac{\sin 2\alpha_0}{4}\right)+V_yR\ln\frac{\cos^2\alpha_n}{\cos\alpha_0\cos\theta}\\
&\quad+V_yR(\cos\alpha_0+\cos\theta-2\cos\alpha_n)+\left(h_0v_0-V_yR\theta+V_yR\alpha_m\right)\\
&\quad\left\langle 2\alpha_n-\alpha_0-\theta+\frac{1}{M}\ln\frac{\tan^2(\pi/4+\alpha_n/2)}{\tan(\pi/4+\alpha_0/2)\tan(\pi/4+\theta/2)}+\frac{2\sqrt{M^2-1}}{M}\cdot\right.\\
&\quad\left\{\arctan\left[\sqrt{\frac{M+1}{M-1}}\tan\left(\frac{\alpha_0}{2}\right)\right]-2\arctan\left[\sqrt{\frac{M+1}{M-1}}\tan\left(\frac{\alpha_n}{2}\right)\right]\right.\\
&\quad\left.\left.+\arctan\left[\sqrt{\frac{M+1}{M-1}}\tan\left(\frac{\theta}{2}\right)\right]\right\}\right\rangle.
\end{aligned} \tag{24}$$

Substituting Eqs. (22) and (24) into Eq. (21) yields the friction power

$$
\begin{aligned}
\dot{W}_{\mathrm{uf}} = 4mkw\Big\langle & v_R R(\alpha_0+\theta-2\alpha_n) + V_y R \ln\frac{\cos^2\alpha_n}{\cos\alpha_0\cos\theta} \\
& + V_y R(\cos\alpha_0+\cos\theta-2\cos\alpha_n) + \frac{2(U/w - V_y R\theta + V_y R\alpha_m)}{M\sqrt{M^2-1}} \\
& \left\{ 2\arctan\left[\sqrt{\frac{M+1}{M-1}}\tan\left(\frac{\alpha_n}{2}\right)\right] - \arctan\left[\sqrt{\frac{M+1}{M-1}}\tan\left(\frac{\theta}{2}\right)\right],\right. \\
& - \arctan\left[\sqrt{\frac{M+1}{M-1}}\tan\left(\frac{\alpha_0}{2}\right)\right] \\
& \left. + \frac{\sqrt{M^2-1}}{2}\ln\frac{\tan^2(\pi/4+\alpha_n/2)}{\tan(\pi/4+\alpha_0/2)\tan(\pi/4+\theta/2)}\right\}\Big\rangle.
\end{aligned}
\tag{25}
$$

3.4 Tension Power

If there are front tension σ_{f} and back tension σ_{b} effects on the workpiece, the tension power of the deformation zone is

$$
\dot{W}_{\mathrm{uT}} = 4(\sigma_{\mathrm{b}} w h_0 v_0 - \sigma_{\mathrm{f}} w h_1 v_1) = 4U(\sigma_{\mathrm{b}} - \sigma_{\mathrm{f}}). \tag{26}
$$

3.5 Total Power Functional

According to Eqs. (12), (17), (25) and (26), the total power functional model in the upward rolling based on the first variation principle of a rigid-plastic material is defined as Eq. (27) [27].

$$
J_{\mathrm{u}}^{*} = \dot{W}_{\mathrm{ui}} + \dot{W}_{\mathrm{us}} + \dot{W}_{\mathrm{uf}} + \dot{W}_{\mathrm{uT}}. \tag{27}
$$

By solving the differential of the total power functional J_{u}^{*} in Eq. (27) with respect to the arbitrary variable α_n and making it equal to zero [28], the following equation can be obtained

$$
\frac{\mathrm{d}J_{\mathrm{u}}^{*}}{\mathrm{d}\alpha_n} = \frac{\mathrm{d}\dot{W}_{\mathrm{ui}}}{\mathrm{d}\alpha_n} + \frac{\mathrm{d}\dot{W}_{\mathrm{us}}}{\mathrm{d}\alpha_n} + \frac{\mathrm{d}\dot{W}_{\mathrm{uf}}}{\mathrm{d}\alpha_n} + \frac{\mathrm{d}\dot{W}_{\mathrm{uT}}}{\mathrm{d}\alpha_n} = 0, \tag{28}
$$

where

$$
\frac{\mathrm{d}\dot{W}_{\mathrm{ui}}}{\mathrm{d}\alpha_n} = \frac{32}{7}\sigma_{\mathrm{s}} N \ln\frac{h_0}{h_1}, \tag{29}
$$

$$
\frac{\mathrm{d}\dot{W}_{\mathrm{us}}}{\mathrm{d}\alpha_n} = 2kN(\tan\theta + \tan\alpha_0), \tag{30}
$$

$$
\begin{aligned}
\frac{\mathrm{d}\dot{W}_{\mathrm{uf}}}{\mathrm{d}\alpha_n} = 8mkw\Big\langle & -v_R R - V_y R\tan\alpha_n + \frac{U/w - V_y R\theta + V_y R\alpha_m}{\cos\alpha_n(M-\cos\alpha_n)} \\
& + V_y R\sin\alpha_n + \frac{N}{wM\sqrt{M^2-1}}\left\{2\arctan\left[\sqrt{\frac{M+1}{M-1}}\tan\left(\frac{\alpha_n}{2}\right)\right]\right. \\
& - \arctan\left[\sqrt{\frac{M+1}{M-1}}\tan\left(\frac{\alpha_0}{2}\right)\right] - \arctan\left[\sqrt{\frac{M+1}{M-1}}\tan\left(\frac{\theta}{2}\right)\right] \\
& \left. + \frac{\sqrt{M^2-1}}{2}\ln\frac{\tan^2(\pi/4+\alpha_n/2)}{\tan(\pi/4+\alpha_0/2)\tan(\pi/4+\theta/2)}\right\}\Big\rangle.
\end{aligned}
\tag{31}
$$

$$
\frac{\mathrm{d}\dot{W}_{\mathrm{uT}}}{\mathrm{d}\alpha_n} = 4N(\sigma_{\mathrm{b}} - \sigma_{\mathrm{f}}), \tag{32}
$$

where $N = \frac{\mathrm{d}U}{\mathrm{d}\alpha_n} = v_R w R\sin 2\alpha_n - v_R w(h_0 + R\cos\theta)\sin\alpha_n$.

4 Analytical Model of Total Power Functional in Downward Rolling

According to Figure 3, in the downward rolling process, the expressions for the length of the contact arc l_{total} and the thickness of the exit zone h_1 in the deformation zone are defined as Eqs. (33) and (34).

$$l_{\text{total}} = l + x_0 = \sqrt{R^2 - (R\cos\alpha_0 - \Delta h)^2} + x_0, \tag{33}$$

$$h_1 = h_{\text{hthick}} + V_y t, \tag{34}$$

The contact arc in the downward rolling is different from that in the upward rolling, and the deformation zone's length increases in the downward rolling. However, the method used to calculate those powers in the upward rolling can be used in the downward rolling. The internal plastic deformation power can be similarly determined using the MY liner yield criterion. Hence, the mean value of $\cos\alpha$ in deformation zone is obtained as

$$\overline{\cos\alpha} = \frac{\int_{-\alpha_0}^{\theta}\cos\alpha\,\mathrm{d}\alpha}{\theta+\alpha_0} = \frac{\sin\theta + \sin\alpha_0}{\theta+\alpha_0}. \tag{35}$$

The internal plastic deformation power $\dot{W}_{\text{di}}$ becomes

$$\begin{aligned}\dot{W}_{\text{di}} &= \frac{32}{7}\sigma_s \int_{-x_0}^{l}\int_0^w\int_0^{h_x}\left(\frac{-h_0 v_0 + V_y R\theta - V_y R\alpha}{h_x^2}h_x^{'} + \frac{V_y R}{x h_x}h_x^{'}\right)\mathrm{d}x\mathrm{d}y\mathrm{d}z \\ &= \frac{32}{7}\sigma_s U \ln\frac{h_0}{h_1} + \frac{32}{7}\sigma_s w V_y R\left\{\theta\ln\frac{h_1(M-\cos\theta)}{h_0}\right. \\ &\left.+\alpha_0\ln(M-\cos\alpha_0) - (\theta+\alpha_0)\left[1+\ln\left(M - \frac{\sin\theta+\sin\alpha_0}{\theta+\alpha_0}\right)\right]\right\}.\end{aligned} \tag{36}$$

The shear powers at the inlet and exit of the zones are calculated, and then the total shear power is

$$\begin{aligned}\dot{W}_{\text{ds}} &= 2kU(\tan\theta + \tan\alpha_0) - \frac{2kwh_0 V_y R\tan\theta}{l} \\ &- 2kwV_y R\tan\alpha_0\left(-\frac{h_1}{x_0} + \theta + \alpha_0\right).\end{aligned} \tag{37}$$

There is still a length x_0 in the rolling direction when the workpiece exceeds the lowest point of the upper roll in the deformation zone. The mean value of the contact angle α_m in the downward rolling is similarly obtained using the integral mean value theorem

$$\alpha_m = \frac{\int_{-x_0}^{l}\alpha\,\mathrm{d}x}{l+x_0} = \frac{\theta\sin\theta + \cos\theta - \alpha_0\sin\alpha_0 - \cos\alpha_0}{\sin\theta + \sin\alpha_0}. \tag{38}$$

The friction power $\dot{W}_{\text{df}}$ is

$$\begin{aligned}\dot{W}_{\text{df}} &= 4mkw\left(\int_{-x_0}^{l}|\Delta v_x|\cos\alpha\sec\alpha\,\mathrm{d}x + \int_{-x_0}^{l}|\Delta v_y|\sin\alpha\sec\alpha\,\mathrm{d}x\right) \\ &= 4mkw\left\langle v_R R\left(\theta - 2\alpha_n - \frac{\sin 2\alpha_0}{2}\right) + V_y R\left(\ln\frac{\cos^2\alpha_n\cos\alpha_0}{\cos\theta}\right)\right. \\ &- V_y R(2\cos\alpha_n - \cos\theta - \cos\alpha_0) + \frac{2(U/w - V_y R\theta + V_y R\alpha_m)}{M\sqrt{M^2-1}} \\ &\left\{(2M^2-1)\arctan\left[\sqrt{\frac{M+1}{M-1}}\tan\left(\frac{\alpha_0}{2}\right)\right] - \arctan\left[\sqrt{\frac{M+1}{M-1}}\tan\left(\frac{\theta}{2}\right)\right]\right. \\ &- \alpha_0 M\sqrt{M^2-1} + 2\arctan\left[\sqrt{\frac{M+1}{M-1}}\tan\left(\frac{\alpha_n}{2}\right)\right] \\ &\left.\left.+\frac{\sqrt{M^2-1}}{2}\ln\frac{\tan^2(\pi/4+\alpha_n/2)\tan(\pi/4-\alpha_0/2)}{\tan(\pi/4+\theta/2)}\right\}\right\rangle.\end{aligned} \tag{39}$$

The tension power $\dot{W}_{\text{dT}}$ is

$$\dot{W}_{\text{dT}} = 4U(\sigma_b - \sigma_f). \tag{40}$$

According to Eqs. (36), (37), (39) and (40), the total power functional model in the downward rolling is

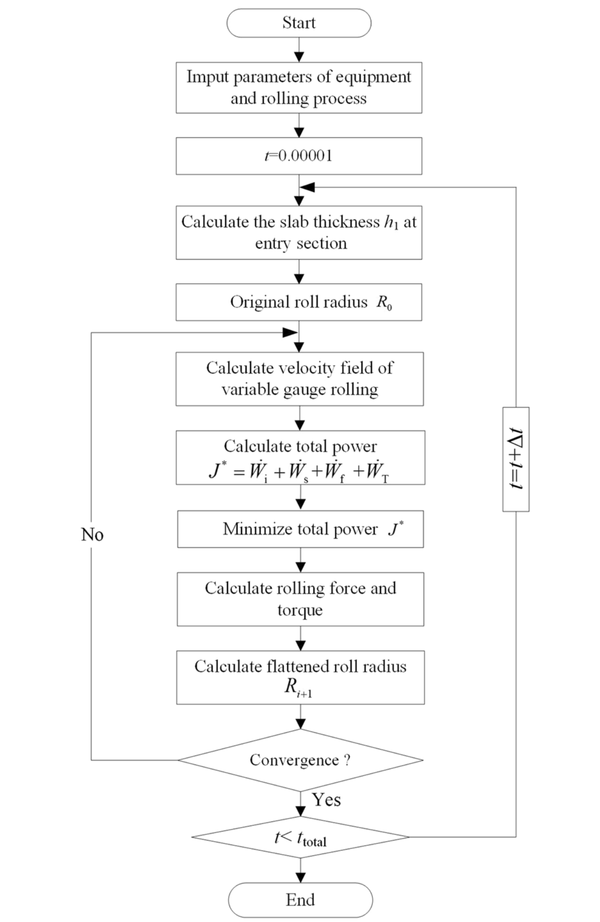

Figure 4 Flowchart of the calculation in variable gauge rolling

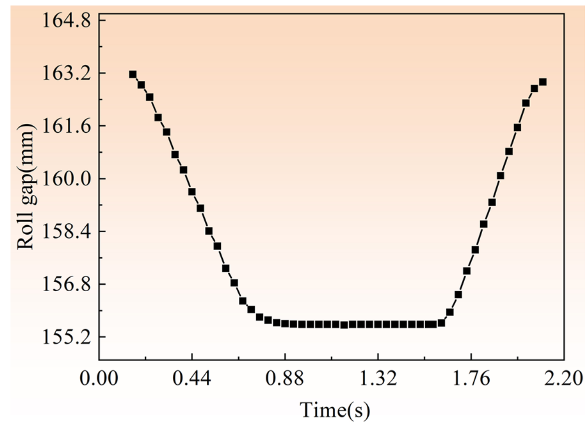

Figure 5 Variation of roll gap with time in MAS rolling

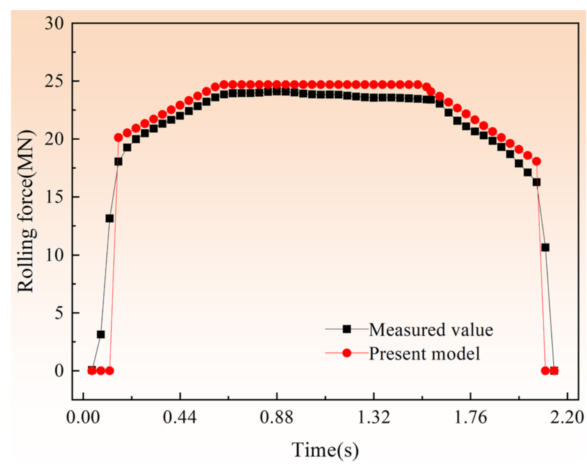

Figure 6 Comparison of roll separating force for theoretical and measured values in MAS rolling

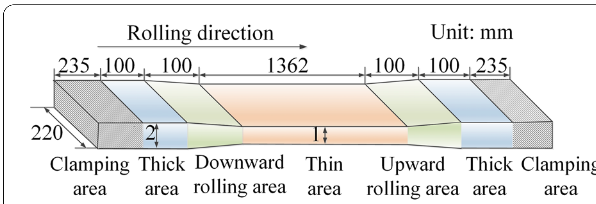

Figure 7 Geometry dimension of the workpiece after rolling

$$J_{\mathrm{d}}^{*} = \dot{W}_{\mathrm{di}} + \dot{W}_{\mathrm{ds}} + \dot{W}_{\mathrm{df}} + \dot{W}_{\mathrm{dT}}. \tag{41}$$

By solving the differential of the total power functional in Eq. (41) with respect to the arbitrary variable α_n and making it equal to zero, the following equation can be obtained as

$$\frac{\mathrm{d}J_{\mathrm{d}}^{*}}{\mathrm{d}\alpha_n} = \frac{\mathrm{d}\dot{W}_{\mathrm{di}}}{\mathrm{d}\alpha_n} + \frac{\mathrm{d}\dot{W}_{\mathrm{ds}}}{\mathrm{d}\alpha_n} + \frac{\mathrm{d}\dot{W}_{\mathrm{df}}}{\mathrm{d}\alpha_n} + \frac{\mathrm{d}\dot{W}_{\mathrm{dT}}}{\mathrm{d}\alpha_n} = 0, \tag{42}$$

where

$$\frac{\mathrm{d}\dot{W}_{\mathrm{di}}}{\mathrm{d}\alpha_n} = \frac{32}{7}\sigma_{\mathrm{s}} N \ln \frac{h_0}{h_1}, \tag{43}$$

$$\frac{\mathrm{d}\dot{W}_{\mathrm{ds}}}{\mathrm{d}\alpha_n} = 2kN(\tan\theta + \tan\alpha_0), \tag{44}$$

$$\begin{aligned}\frac{\mathrm{d}\dot{W}_{\mathrm{df}}}{\mathrm{d}\alpha_n} = 8mkw\Big\langle -V_yR\tan\alpha_n + V_yR\sin\alpha_n + \frac{U/w - V_yR\theta + V_yR\alpha_m}{\cos\alpha_n(M-\cos\alpha_n)} \\ -v_RR + \frac{N}{wM\sqrt{M^2-1}}\Big\{\left(2M^2-1\right)\arctan\left[\sqrt{\frac{M+1}{M-1}}\tan\left(\frac{\alpha_0}{2}\right)\right] - \alpha_0 M\cdot \\ \sqrt{M^2-1} - \arctan\left[\sqrt{\frac{M+1}{M-1}}\tan\left(\frac{\theta}{2}\right)\right] + 2\arctan\left[\sqrt{\frac{M+1}{M-1}}\tan\left(\frac{\alpha_n}{2}\right)\right] \\ + \frac{\sqrt{M^2-1}}{2}\ln\frac{\tan^2(\pi/4+\alpha_n/2)\tan(\pi/4-\alpha_0/2)}{\tan(\pi/4+\theta/2)}\Big\}\Big\rangle,\end{aligned} \tag{45}$$

$$\frac{\mathrm{d}\dot{W}_{\mathrm{dT}}}{\mathrm{d}\alpha_n} = 4N(\sigma_{\mathrm{b}} - \sigma_{\mathrm{f}}). \tag{46}$$

5 Results and Discussions

The minimum angle α_n (neutral angle) and the minimum value of the total power $J^*_{\min}$ are obtained in different conditions of the upward and downward rolling based on Eqs. (27), (28), (41) and (42). The analytical models of the roll torque M, roll separating force F, and stress state effect coefficient n_σ could be calculated as Eq.(47) [29].

$$M = \frac{R_0 J^*_{\min}}{2v_R}, F = \frac{M}{\chi\, l_{\mathrm{total}}}, n_\sigma = \frac{F}{4wl_{\mathrm{total}}\,k}. \tag{47}$$

The work roll radius is obviously flattened for the cold variable gauge rolling with front and back tensions, such as TRB rolling. Hitchcock's roll elastic flattening model with consideration of front and back tensions is adopted, and the roll separating force in the elastic zone is calculated based on our previous cold rolling research [30]. The calculation flow chart is depicted in Figure 4.

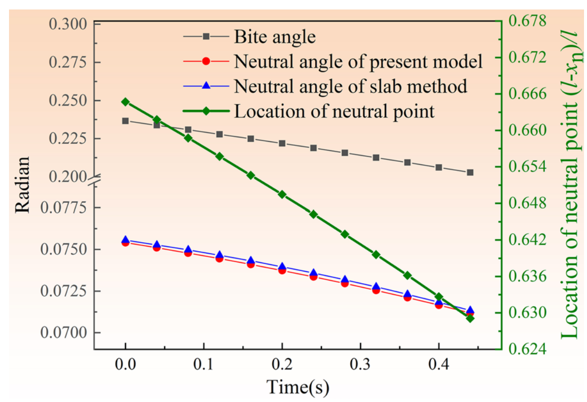

Figure 9 Variations of the bite angle, neutral angle, and location of neutral points in upward rolling

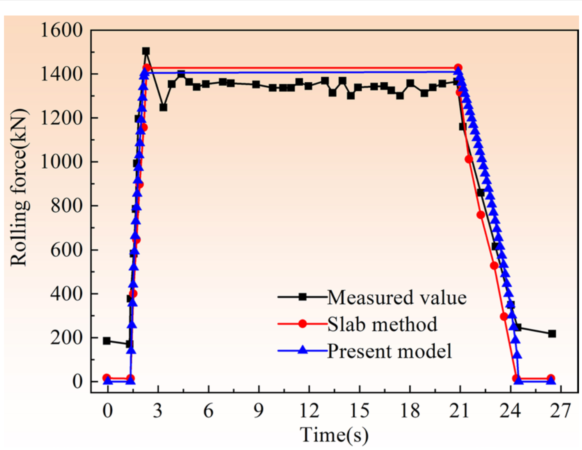

Figure 8 Comparison of roll separating force in a TRB

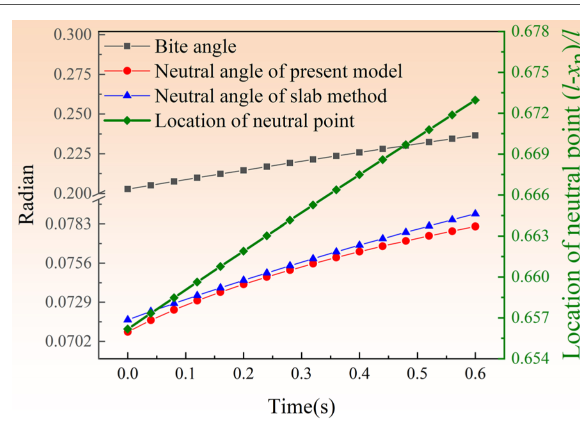

Figure 10 Variations of the bite angle, neutral angle, and location neutral points in downward rolling

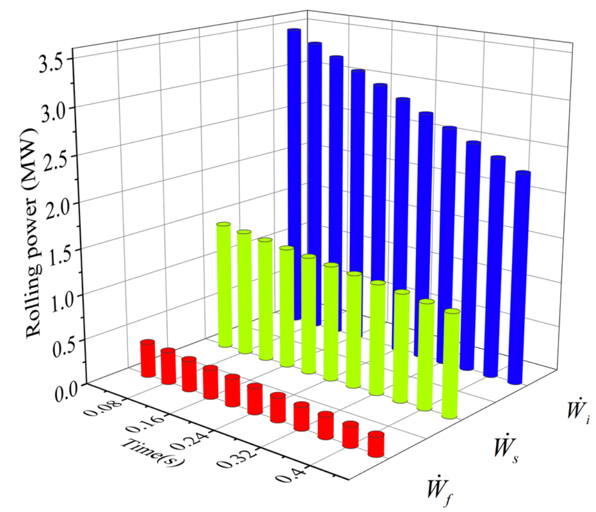

Figure 11 Variation of powers in upward rolling

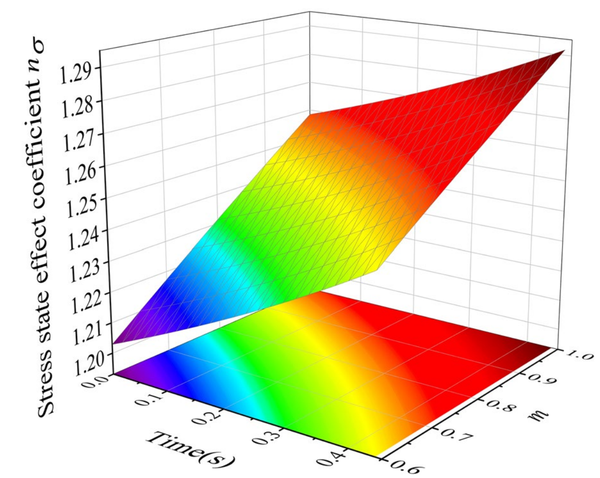

Figure 13 Influence of friction factor on stress state coefficient in upward rolling

The mathematical model used in this research (present model) is certified using the measured data of the MAS rolling process in a medium plate hot rolling plant. The rolling technology is depicted in Figure 1(a). The workpiece material is Q345, the thickness is 0.182 m, and the width is 2.611 m. The roll diameter is 0.946 m, and the roll circumferential speed is 0.951 m/s. The change of the roll gap with time is depicted in Figure 5. The downward rolling process is performed at the head of the workpiece. Then the traditional equal thickness rolling process is carried out at high speed. Finally, the upward rolling process is executed near the end of the workpiece. The roll separating force in this process that is calculated with the present model is contrasted with measured values, as depicted in Figure 6. The maximum deviation is less than 5%, except for the fact that the predicted roll separating force is larger at the starting point of the downward rolling and the endpoint of the upward rolling.

The predicted roll separating force accuracy of the present model in the TRB cold rolling process is verified using Zhang's research [21], in which a high strength micro-alloyed steel CR340 workpiece was rolled by a 450 mm four-high cold rolling mill with hydraulic tension in the laboratory. The workpiece is rolled as shown in Figure 7 (the unit is mm). The original thickness for the

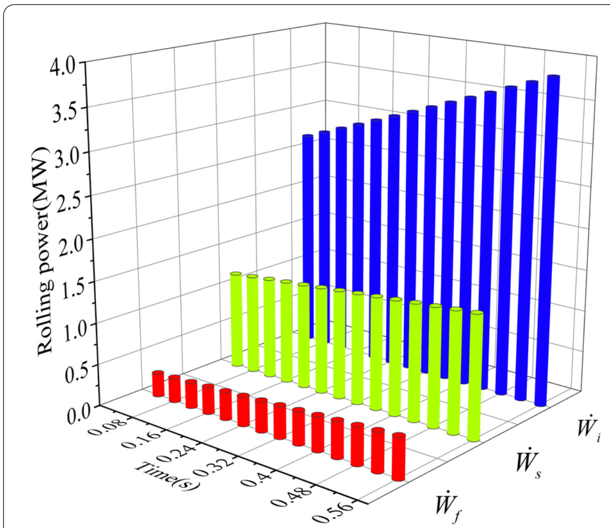

Figure 12 Variation of powers in downward rolling

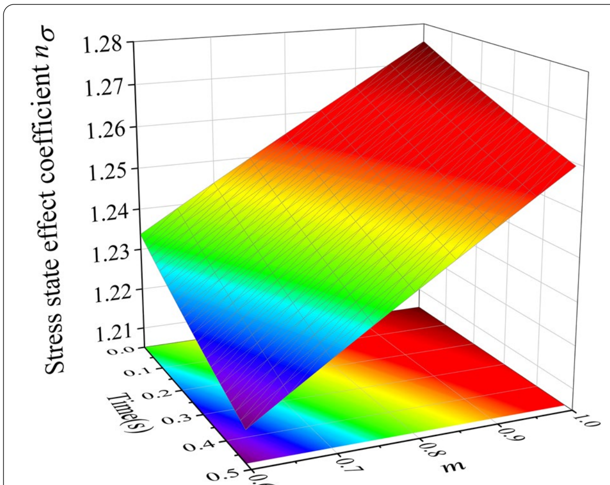

Figure 14 Influence of friction factor on stress state coefficient in downward rolling

workpiece is 2 mm and the front and back tensions are 40 kN.

The roll separating force computed with the present model is contrasted with the measured data in a rolling experiment and the values calculated using the slab method based on the idea of solving the Karman differential equation, as shown in Figure 8. The rolls are flattened and bounced severely due to the large material deformation resistance of the plate in cold rolling. The actual roll gap has to be less than the target roll gap to ensure the finished product size, as indicated in Figure 7. Therefore, the roll separating force is not zero at the beginning of the downward rolling and the end of the upward rolling. The roll separating force computed by the present model is larger than the computed results using the slab method, and it is slightly larger than the measured data. However, the compared results show good agreement, and the present model meets the requirements and accuracy of the roll separating force setting value. Therefore, the mathematical model used in this research can be exploited to forecast the roll separating force and to research variable gauge rolling.

Figures 9 and 10 show the variations of the bite angle, neutral angles, and locations of neutral points with time for upward and downward rolling, using the MAS rolling process parameters illustrated in Figure 5. The variation of the neutral angle in variable gauge rolling is compared with that of the slab method. The neutral angle calculated by the present model is slightly less than that calculated with the slab method because the calculation formula of the neutral angle in the slab method is based on the assumption that the unit pressure is uniformly distributed along the contact arc. The bite and neutral angles decrease, and the decrease rate of the bite angle is more remarkable than that of the neutral angle in upward rolling due to the reduction rate of workpiece gradually decreasing. On the contrary, the bite and neutral angles increase, and the increase rate of bite angle is more significant than that of neutral angle in downward rolling due to the gradual decrease of the reduction rate of the workpiece. According to Figures 9 and 10, the neutral point's location moves toward the inlet of the zone in upward rolling and moves toward the exit of the zone in downward rolling.

The variations of the internal plastic deformation power $\dot{W}_{\mathrm{i}}$, shear power $\dot{W}_{\mathrm{s}}$, and friction power $\dot{W}_{\mathrm{f}}$ with time in upward and downward rolling are depicted in Figures 11 and 12. It can be seen from the figures that the internal plastic deformation and shear powers make up a larger proportion of the total power. In comparison, the friction power makes up a minor proportion. They all increase with time in the upward rolling but decrease with time in the downward rolling. Moreover, the internal plastic deformation power obviously varies with time, while the friction power only changes slightly.

Figures 13 and 14 show that the stress state effect coefficient n_{σ} increases linearly with the increase of the rolling time in upward rolling, while it decreases with the increase of the rolling time in downward rolling using the MAS rolling process parameters displayed in Figure 5. This is because the shape factor of the rolled piece is less than 1; i.e., the ratio of the projected length to the average thickness is less than 1 in the deformation zone. Furthermore, for the deformation of the workpiece during variable gauge rolling, the effect of the external zone should be considered. Deformation not only occurs in the contact zone should be considered but also in the external zone. It is evident from Figures 11 and 12 that the shear power is greater than the friction power; that is to say, the influence of the external zone is the primary influence. Therefore, when the shape factor of the workpiece is small, the shear power is considerable. The external force must be increased to deform the workpiece, and the stress state effect coefficient must correspondingly increase. Figures 13 and 14 also show that the stress state effect coefficient n_{σ} obviously increases linearly with the increase of the friction factor m in the upward and downward rolling.

6 Conclusions

(1) The velocity and the strain rate fields in variable gauge rolling are built with consideration of the influence of the upward or downward motion of the rolls, with this field satisfying kinematically admissible conditions. The analytical models of the roll separating force, roll torque, and stress state effect coefficient are obtained.
(2) Comparisons among the predicted roll separating forces and measured values in MAS rolling in a medium plate hot rolling plant and a TRB rolling experiment show that the analytical model exhibits excellent prediction accuracy. The present model can, therefore, be utilized to research variable gauge rolling.
(3) The bite and neutral angles decrease in the upward rolling and increase in the downward rolling. The neutral point goes toward the inlet of the zone in upward rolling and moves toward the exit of the zone in downward rolling. They are the essential parameters of the micro-tracing strategy, which determines the length of the transition zone of the variable thickness plates.
(4) The stress state effect coefficient increases in the upward rolling and decreases in the downward rolling. The friction factor influences the stress state

effect coefficient noticeably. The thickness control strategy is developed based on the force parameters and the rolling mill bounce equation, which determines the thickness of the transition zone of the variable thickness plates.

Acknowledgements
Not applicable.

Author Contributions
YL, QH and DZ were in charge of the whole trial; ZW and TW wrote the manuscript; JS and XZ assisted with result analyses. All authors read and approved the final manuscript.

Authors' Information
Yuanming Liu, born in 1988, is currently an associate professor at *Engineering Research Center of Advanced Metal Composites Forming Technology and Equipment, Ministry of Education, Taiyuan University of Technology, China*. His main research interests include rolling process of plate and strip, and mathematical model of rolling process control.
Zhenhua Wang, born in 1990 is currently a lecturer at *Engineering Research Center of Advanced Metal Composites Forming Technology and Equipment, Ministry of Education, Taiyuan University of Technology, China*. His main research interest is intelligent research of rolling process.
Tao Wang, born in 1985, is currently a professor and a PhD candidate supervisor at *Engineering Research Center of Advanced Metal Composites Forming Technology and Equipment, Ministry of Education, Taiyuan University of Technology, China*. His main research interests include rolling process and equipment.
Jie Sun, born in 1984, is currently a professor and a PhD candidate supervisor at *State Key Laboratory of Rolling and Automation, Northeastern University, China.* His main research interests include automation and intelligent research of rolling process.
Xianguang Zheng, born in 1998, is currently a master candidate at *Engineering Research Center of Advanced Metal Composites Forming Technology and Equipment, Ministry of Education, Taiyuan University of Technology, China.* His main research interest is variable gauge rolling process.
Dianhua Zhang, born in 1963, is currently a professor and a PhD candidate supervisor at *State Key Laboratory of Rolling and Automation, Northeastern University, China.* His main research interests include automation and intelligent research of rolling process.
Qingxue Huang, born in 1960, is currently an Academician of Chinese Academy of Engineering, a professor and a PhD candidate supervisor at *Engineering Research Center of Advanced Metal Composites Forming Technology and Equipment, Ministry of Education, Taiyuan University of Technology, China*. His main research interests include modern rolling process and equipment design theory.

Funding
Supported by National Natural Science Foundation of China (Grant Nos. 51904206, 52105390, 51974196, 51805359), Open Research Fund from the State Key Laboratory of Rolling and Automation, Northeastern University (Grant No. 2020RALKFKT011), Shanxi Province Science and Technology Major Projects (Grant No. 20181102015), China Postdoctoral Science Foundation (Grant No. 2020M670705).

Competing Interests
The authors declare no competing financial interests.

Author Details
[1]College of Mechanical and Vehicle Engineering, Taiyuan University of Technology, Taiyuan 030024, China. [2]Engineering Research Center of Advanced Metal Composites Forming Technology and Equipment, Ministry of Education, Taiyuan 030024, China. [3]TYUT-UOW Joint Research Center, Taiyuan University of Technology, Taiyuan 030024, China. [4]State Key Laboratory of Rolling and Automation, Northeastern University, Shenyang 110819, China.

Received: 15 January 2022 Revised: 12 May 2022 Accepted: 1 June 2022
Published online: 07 July 2022

References
[1] X H Liu. Prospects for variable gauge rolling: technology, theory and application. *J. Iron Steel Res. Int.*, 2011, 18(1): 1-7.
[2] Y Zhi, X G Wang, S Wang, et al. A review on the rolling technology of shape flat products. *Int. J. Adv. Manuf. Tech.*, 2018, 94(9-12): 4507-4518.
[3] Y B Yang, Y Peng. Dynamic rolling model based on uniform deformation. *J. Manuf. Process*, 2020, 58: 1334-1347.
[4] S Wang, X G Wang, X H Liu, et al. Experiment and simulation of variable thickness rolling for 3D-profiled blank. *J. Mater. Process Tech.*, 2021, 290: 116971.
[5] D Y Yang, M Bambach, J Cao, et al. Flexibility in metal forming. *Cirp Ann.-Manuf. Techn.*, 2018, 67(2): 743-765.
[6] X G Wang, S Wang, X H Liu. Variable thickness rolling of plates thick in the middle and thin on the sides. *J Mater Process Tech*, 2020, 277: 116432.
[7] D C Wang, H M Liu, J Liu. Research and development trend of shape control for cold rolling strip. *Chinese Journal of Mechanical Engineering*, 2017, 30(5): 1248-1261.
[8] T Wang, Q X Huang, H Xiao, et al. Modification of roll flattening analytical model based on the plane assumption. *Chinese Journal of Mechanical Engineering*, 2018, 31: 46.
[9] T Yanazawa, J Miyoshi, K Tsubota, et al. Development of a new plan view pattern control system in plate rolling. *Kawasaki Steel Technical Report*, 1980, 1(9): 41-42.
[10] R Kopp. Some current development trends in metal-forming technology. *J. Mater. Process Tech.*, 1996, 60(1-4): 1-9.
[11] Y Fukumoto, M Nagai. Steel bridges: new steels and innovative erection methods. *Progress in Structural Engineering and Materials*, 2000, 2(1): 34-40.
[12] J S Wang, Z Y Jiang, A K Tieu, et al. A flying gauge change model in tandem cold strip mill. *J. Mater. Process Tech.*, 2008, 204(1-3): 152-161.
[13] F W Zhu, X L Hu, Z Zhao, et al. Analysis of process control model of plate MAS rolling. *J. Iron Steel Res. Int.*, 2010, 17(4): 31-33.
[14] D Kim, J Kim, Y Lee, et al. Study of residual stresses in tailor rolled blanked Al5J32-T4 sheets. *Rare Metals*, 2006, 25(6): 111-117.
[15] A Meyer, B Wietbrock, G Hirt. Increasing of the drawing depth using tailor rolled blanks-numerical and experimental analysis. *Int. J. Mach. Tool Manu.*, 2008, 48(5): 522-531.
[16] C S Ding, X Y Cui, G Y Li. Accurate analysis and thickness optimization of tailor rolled blanks based on isogeometric analysis. *Struct. Multidiscip O*, 2016, 54(4): 871-887.
[17] Y Zhi, X H Liu, T Sun, et al. Investigation of mathematical model for the transition zone of tailor rolled blank for variable gauge rolling. *Journal of Harbin Engineering University*, 2017, 38(4): 602-609. (in Chinese)
[18] D C Wang, L C Dong, H M Liu, et al. Velocity preset and transitional zone's shape optimization for tailor rolled blank. *J. Iron Steel Res. Int.*, 2015, 22(4): 279-287.
[19] W Yu, G J Sun. Forward slip theoretical model and simulation for variable gauge rolling of TRB sheet. *J. Univ. Sci. Technol. B*, 2014, 36(2): 241-245. (in Chinese)
[20] Y Zhang, J Tan. Numerical simulation and vertical motion control of rolls for variable gauge rolling. *J. Iron Steel Res. Int.*, 2015, 22(8): 703-708.
[21] G J Zhang. Research on rolling theory and experiment for longitudinally variable gauge cold rolling. Xi'an: Northeastern University, 2011. (in Chinese)
[22] H L Yu, K Tieu, C Lu, et al. The wave motion of the rolling force during variable gauge rolling. *Steel Res. Int.*, 2013, 84(12): 1203-1208.
[23] X H Liu, Q L Zhao, L Z Liu. Recent development on theory and application of variable gauge rolling: A review. *Acta Metall. Sin.*, 2014, 27(3): 483-493.
[24] Y M Liu, G S Ma, D W Zhao, et al. Analysis of hot strip rolling using exponent velocity field and MY criterion. *Int. J. Mech. Sci.*, 2015, 98: 126-131.
[25] D H Zhang, Y M Liu, J Sun, et al. A novel analytical approach to predict rolling force in hot strip finish rolling based on cosine velocity field and equal area criterion. *Int. J. Adv. Manuf. Tech.*, 2016, 84(5-8): 843-850.
[26] Y M Liu, J Sun, D H Zhang, et al. Three-dimensional analysis of edge rolling based on dual-stream function velocity field theory. *J. Manuf. Process*, 2018, 34(1): 349-355.

[27] B X Yang, H J Xu, Q An. Analysis of 3D plastic deformation in vertical rolling based on global weighted velocity field. *Int. J. Adv. Manuf. Tech.*, 2022 120: 6647–6659.
[28] Y M Liu, P J Hao, T Wang, et al. Mathematical model for vertical rolling deformation based on energy method. *Int. J Adv. Manuf. Tech.*, 2020, 107: 875-883.
[29] Y M Liu, Z H Wang, T Wang, et al. Prediction and mechanism analysis of the force and shape parameters using cubic function model in vertical rolling. *J. Mater. Process Tech.*, 2022, 303: 117500.
[30] Y M Liu, J Sun, Q L Wang, et al. Mathematical model for cold rolling based on energy method. *Meccanica*, 2017, 52(9): 2069-2080.